Materials Science & Engineering A 892 (2024) 146068

Contents lists available at ScienceDirect

Materials Science & Engineering A

journal homepage: www.elsevier.com/locate/msea

Heat treatment effects on microstructure and properties of Cu–Ti–Fe alloys

Gang'ao Xin [a], Meng Zhou [a,**], Ke Jing [a], Haoyan Hu [a], Zheng'ao Li [a], Yi Zhang [a,*], Qian Bai [b], Caijiao Tian [a], Baohong Tian [a], Xu Li [c], Alex A. Volinsky [d], Jin Zou [e,***]

[a] School of Materials Science and Engineering, Henan University of Science and Technology, Provincial and Ministerial Co-construction of Collaborative Innovation Center for Non-ferrous Metals New Materials and Advanced Processing Technology, Luoyang, 471023, PR China
[b] Medical Research Center, The Second Affiliated Hospital of Zhengzhou University, Zhengzhou, 450014, PR China
[c] Center for Advanced Measurement Science, National Institute of Metrology, Beijing, 100029, PR China
[d] Department of Mechanical Engineering, University of South Florida, 4202 E. Fowler Ave. ENG 030, Tampa, 33620, USA
[e] Jiangxi Key Laboratory for Advanced Copper and Tungsten Materials, Jiangxi Academic of Sciences, Nanchang, 330096, PR China

ARTICLE INFO

Keywords:
Copper alloys
Aging treatment
Mechanical properties
Microstructure
Precipitation strengthening

ABSTRACT

High-strength Cu–Ti–Fe alloys were prepared and investigated in this study. The alloy was subjected to cold deformation and aging treatment, and revealed the transformation mechanism of the microstructure and properties. Cold deformation of 60 %, aging at 450 °C for 240 min, can optimize the hardness and conductivity of the Cu–Ti–Fe alloy. The hardness and electrical conductivity of Cu-1.5Ti-0.3Fe alloy increased from 196.8 HV to 7.8 % IACS to 269.3 HV and 19.8 % IACS after aged. Cu_4Ti and Fe_2Ti are the mainly precipitated phases in Cu–Ti–Fe alloy, which effectively obstructs dislocations slipping and delays recrystallization, and the most important strengthening mechanism. The concentration of solute atoms increased could further improve the grain boundary strengthening, solution strengthening, and deformation strengthening.

1. Introduction

Copper alloys have excellent characteristics such as high strength, and high thermal and electrical conductivity [1–3]. Copper alloys play an irreplaceable role in machinery manufacturing, marine transportation, lead frames, the electronic industry, medical equipment, and other fields [4–7]. As industrial development continues to move towards electrification and new energy, the demand for copper alloys has increased, which also puts higher requirements on their performance [8]. In order to further improve the performance of copper alloys, different alloying elements are added to the copper matrix to adjust the alloy properties through solution and precipitation strengthening and improve the strength and conductivity of the alloy [9].

In order to meet specific application needs, different copper alloys have been developed, such as Cu-Be [10], Cu-Ti [11], Cu-Ni-Si [12], Cu-Cr-Zr [13] and Cu–Fe–P [14] and so on. Among them, Cu–Be alloy is a typical precipitation-reinforced copper alloy, which has excellent mechanical properties, wear resistance, and good electrical conductivity, and is widely used in the electronics and aerospace fields [15,16]. However, Cu–Be alloy has poor stress relaxation resistance at high temperatures. The new concepts of green development, the non-toxic characteristics, harmless use, and recycling have received more attention. Due to the high carcinogenicity of the Be element, the use of Cu–Be alloys has been gradually limited.

Therefore, different copper alloys have been developed to replace the Cu–Be alloys. Among them, Cu–Ti alloy has attracted wide attention for its high strength and elasticity, good welding performance and fatigue resistance, and is regarded as the most likely alloy to replace Cu–Be alloy [17,18]. In addition, Jiao et al. found a simple method to extract Ti from alloys, which will also make the recycling of alloys simple [19]. Cu–Ti alloy is a precipitation-strengthened copper alloy, and β'-Cu_4Ti is considered to be its important strengthening phase. Usually at longer aging, β'-Cu_4Ti will transform into β-Cu_3Ti, and the precipitated phase will change from a co-lattice metastable state to a non-co-lattice equilibrium state [20,21]. The tensile strength of Cu–Ti alloy with high Ti content in aged state is comparable to the Cu–Be alloy, but when the Ti content is greater than 4.5 wt%, the water quenching process cannot completely keep Ti in the solid solution, which makes the formability of

* Corresponding author.
** Corresponding author.
*** Corresponding author.
E-mail addresses: zhoumeng0902@126.com (M. Zhou), zhshgu436@163.com (Y. Zhang), niatzou@126.com (J. Zou).

https://doi.org/10.1016/j.msea.2023.146068
Received 9 October 2023; Received in revised form 22 December 2023; Accepted 31 December 2023
Available online 1 January 2024
0921-5093/

the alloy poor [22,23]. In order to further optimize the comprehensive properties of Cu–Ti alloys, many scholars have tried to add a third element to the alloy, such as: Cr [24], Al [25], Mg [26], Fe [27] and so on. In the 90s, studies pointed out that Ti and Fe have similar properties and can be precipitated from the matrix in the form of FeTi [28,29]. Some scholars have studied Cu–Fe–Ti alloys with different element content, and found that FeTi or Fe_2Ti phases can precipitate, cold deformation can promote precipitation, and precipitated phases can pin dislocations and slow down the recrystallization [30–32]. Rouxel et al. found that adding a trace amount of Fe to Cu–Ti alloy can improve its strength after aging to a certain extent, and maintain good formability in the solid solution state [33]. However, at present, there are few micro-alloying studies of the Cu–Ti alloys with low Ti content, and the influence of the third element on the properties and microstructure changes of the alloy needs further study.

In this article, we introduce two novel alloys, namely Cu-1.5Ti-0.3Fe and Cu-1.5Ti-0.5Fe, and investigate an appropriate heat treatment method for Cu–Ti–Fe alloys. By accurately controlling multiple test variables, the effects of alloy composition, cold deformation and aging temperature on alloy properties were analyzed. Electron backscatter diffraction (EBSD), transmission electron microscopy (TEM), high-resolution transmission electron microscopy (HRTEM) and other methods were used to study the mechanical properties, microstructure and precipitated phases after alloy deformation and heat treatment. The strength and electrical conductivity of the alloy have been greatly improved through process optimization.

2. Materials and methods

In this test, 5 kg of Cu–Ti–Fe alloy ingots with different iron content were prepared, and the raw materials were high-purity electrolytic copper metal, Cu–10%Fe intermediate alloy and high-purity sponge titanium particles. The raw materials were cut into small pieces, proportionally placed into a graphite crucible, heated and melted using a vacuum medium-frequency induction furnace. In order to ensure the quality of alloy preparation, argon was introduced during the melting process to prevent the alloy oxidation. For raw materials that oxidize easily, the mass proportion can be appropriately increased to ensure that the smelted specimen is closer to the design composition. In addition, a certain deoxidizer should be added during the alloy melting process, which can react with the impurity elements in the alloy to reduce the impurities. After sampling the middle part of the ingot, the sample composition was obtained by Optima 2100 DV inductively coupled plasma atomic emission spectrometer, and the results are listed in Table 1.

To eliminate compositional segregation during the alloy solidification, the ingots were heated to 880 °C and held for 2 h, after which they were hot rolled into a cylinder with a 43 mm diameter. The rolled sample was cut into a 2 mm × 15 mm × 150 mm plate by wire cutting for the next step. Combined with the actual production of the copper alloy, the treatment process is shown in Fig. 1. OTF-1200X vacuum tube furnace was used for subsequent heat treatment of the samples. The thin plate specimen was heated to 920 °C for 60 min. During the whole process, argon was purged to protect the specimen and prevent surface oxidation. After the heat treatment, the sample was quickly placed into 20 °C water for rapid cooling, so that the Ti and Fe atoms in the alloy did not have enough time to precipitate, obtaining a supersaturated solid solution. The MSK-5070-AC rolling mill was used to cold deform the solid solution sample by 60 % to obtain a sample with a thickness of 0.8 mm. Cold rolling is performed to deform and strengthen the alloy and to thin the specimen by 0.1 mm each time in the same rolling direction. Finally, samples with two types of deformation (undeformed and 60 % cold deformed) were aged at different temperatures. The selection of aging temperature should refer to the previous relevant studies, combined with the alloy phase diagram, to select the temperature range for easy Ti and Fe precipitation [34]. Therefore, the selected aging temperature was 400 °C, 450 °C, 500 °C, and 550 °C, and the aging time was 15–480 min.

Table 1
Chemical composition of the Cu-1.5Ti-0.3Fe and Cu-1.5Ti-0.5Fe alloys in wt.%.

Alloys	Cu	Ti	Fe
Cu-1.5Ti-0.3Fe	Bal.	1.5	0.28
Cu-1.5Ti-0.5Fe	Bal.	1.52	0.5

The hardness of the specimen was tested using the HVS-1000A digital microhardness tester and measured according to the Vickers hardness standard. Prior to hardness measurements, the specimens were polished with 400–2000 grit sandpaper. The downforce of the hardness tester was 500 gf, and the holding time was 15 s. In order to ensure the accuracy of the test results, each specimen was tested 6 times at different positions, and the average value was taken as the hardness of the sample. The electrical conductivity tests used the Sigma2008B digital eddy current metal conductivity meter to measure the international annealed copper standard conductivity (IACS). Each specimen was tested 5 times, and the average value was taken as the electrical conductivity of the specimen. The JSM-IT100 scanning electron microscope was used to observe the microstructure of the alloy. EBSD and EDS results were obtained using the JSM-7800F field emission scanning electron microscope. For the EBSD analysis, the specimens were mechanically polished until their surface was scratch-free, and then electrolytically polished in a solution with 50 % CH_3CH_2OH and H_3PO_4. The voltage of the DC power supply was 5 V, the electrolysis time was 60 s, and the sample was placed into the CH_3CH_2OH solution for ultrasonic cleaning for 3 min after the electrolysis was completed. Electrolytic polishing removes the stress layer on the specimen surface due to mechanical polishing, resulting in more accurate crystallographic data for EBSD analysis. The metal specimen was mechanically ground and then subjected to ion milling with the Gatan 695 ion thinning instrument, followed by TEM analysis using ZEISS' LIBRA-200FE transmission electron microscope.

3. Results

3.1. Mechanical properties and electrical conductivity

In order to meet the needs of practical applications in industrial production, alloys are usually aged [35,36]. In order to explore an aging process suitable for Cu–Ti–Fe alloys, it was treated with a combination of solid solution quenching, cold deformation, and aging. The best properties of the Cu-1.5Ti-0.3Fe and Cu-1.5Ti-0.5Fe alloys were explored at different strains of cold deformation (0 %, 60 %), different aging temperatures (400 °C, 450 °C, 500 °C, 550 °C), and different aging times (15–480 min). The effects of trace iron on the properties and microstructure of the alloy were compared. Fig. 2 shows the mechanical properties and conductivity of the Cu-1.5Ti-0.3Fe and Cu-1.5Ti-0.5Fe alloys at different aging states. In order to explore the effects of cold deformation on the properties of Cu–Ti–Fe alloys after aging, the hardness and electrical conductivity of the Cu-1.5Ti-0.3Fe and Cu-1.5Ti-0.5Fe alloys with different deformation amounts and different aging states are shown in Fig. 2(a) and (d), respectively.

It can be seen from Fig. 2(a) that compared with the sample without cold deformation, the hardness of the Cu-1.5Ti-0.3Fe alloy has been greatly improved after cold deformation and aging. This is because cold deformation introduces a large number of dislocations, which enhances the deformation resistance, thereby forming the deformation strengthening effect. After cold deformation, the hardness of the alloy after aging has an obvious increase trend, while the overall conductivity is only slightly improved, which basically remains stable. The Cu-1.5Ti-0.3Fe alloy with a 60 % cold deformation has the highest hardness after 1 h aging at 500 °C of 275.1 HV, and has the 21.6 % IACS highest conductivity after 8 h aging at 450 °C. The maximum hardness of an alloy with a cold deformation of 0 % after aging is 217 HV.

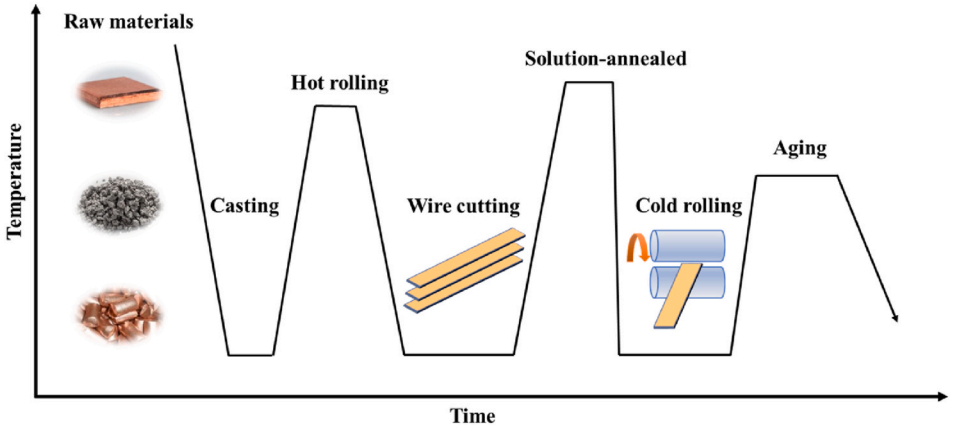

Fig. 1. Processing of Cu–Ti–Fe alloys.

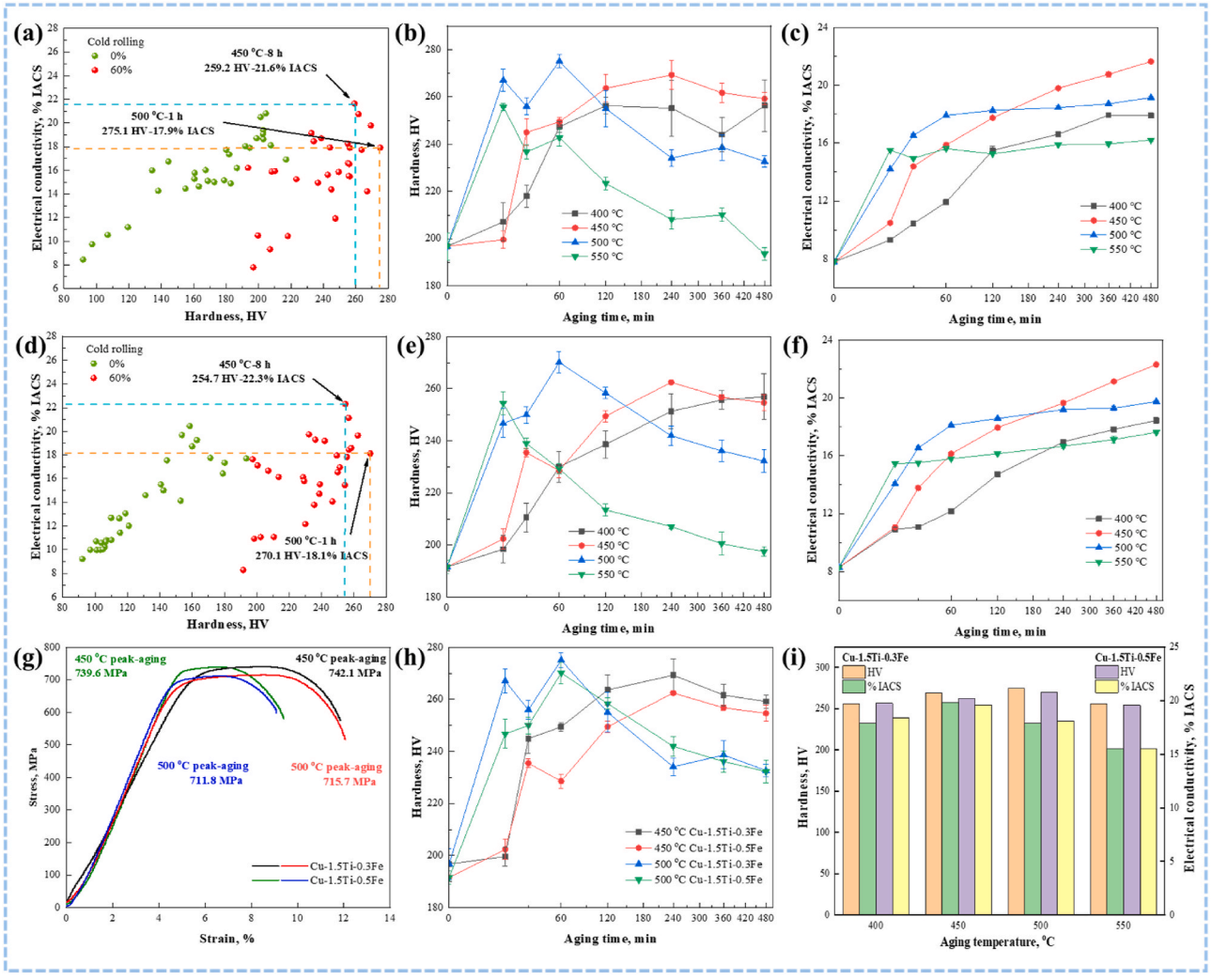

Fig. 2. Mechanical properties and conductivity of the Cu-1.5Ti-0.3Fe and Cu-1.5Ti-0.5Fe alloys: (a) The hardness and conductivity of Cu-1.5Ti-0.3Fe alloy before and after cold rolling; (b, c) Hardness and electrical conductivity of the 60 % cold rolled Cu-1.5Ti-0.3Fe alloy; (d) The hardness and conductivity of Cu-1.5Ti-0.5Fe alloy before and after cold rolling; (e, f) Hardness and electrical conductivity of the 60 % cold rolled Cu-1.5Ti-0.5Fe alloy; (g) Engineering stress-strain curves of the Cu-1.5Ti-0.3Fe and Cu-1.5Ti-0.5Fe alloys; (h) Hardness of the 60 % cold rolled Cu-1.5Ti-0.3Fe and Cu-1.5Ti-0.5Fe alloys; (i) Peak aging hardness and conductivity of the 60 % cold rolled Cu-1.5Ti-0.3Fe and Cu-1.5Ti-0.5Fe alloys.

Fig. 2(b and c) show the hardness and electrical conductivity curves with aging time of the Cu-1.5Ti-0.3Fe alloy with 60 % cold deformation. From the hardness change curve in Fig. 2(b), the three stages of under-aging, peak aging and obsolescence can be clearly seen, among which the peak hardness of the 400 °C, 450 °C, 500 °C and 550 °C aging process is 256.3 HV, 269.3 HV, 275.1 HV and 255.7 HV, respectively. Taking the

hardness curve of the 500 °C aging process as an example, the first 60 min is the under-aging stage, in which the hardness rises rapidly and peaks at 60 min. After 60 min, it is called the over-aging phase, which gradually decreases the hardness of the alloy with aging time. The formation of these three stages is related to the release of elastic distortion energy inside the alloy, the redistribution of dislocations, the precipitation of solute atoms, the formation of secondary phases, and the recrystallization and the growth of grains during the aging process. It takes shorter time for the alloy to reach peak hardness with the aging temperature increase. This is because the higher aging temperature increases the diffusion rate of the atoms, and the Ti atoms in the matrix are easier to precipitate in a short time to form a secondary phase, so that the hardness of the alloy reaches its peak faster.

The electrical conductivity of the alloy gradually increases with aging time in Fig. 2(c). Moreover, the higher the aging temperature, the more rapidly the conductivity increases in the under-aging phase. In the aging process of 400 °C, 450 °C, 500 °C and 550 °C, the corresponding conductivity is 17.9 % IACS, 19.8 % IACS, 17.9 % IACS and 15.5 % IACS. In the aging process, Ti atoms soluble in the matrix are continuously precipitated to form a secondary phase, which reduces the lattice distortion in the matrix and reduces the resistance of electron movement, thereby improving the conductivity. The decrease in conductivity after the too-high aging temperature of 550 °C may be related to the redissolution of solute atoms.

Fig. 2(d) shows the hardness-conductivity diagram of the Cu-1.5Ti-0.5Fe alloy at different aging states, and the overall pattern shows the same trend compared with Fig. 2(a), where cold deformation has a significant effect on the hardness of the alloy after aging, but has little effect on the conductivity. The overall hardness of the Cu-1.5Ti-0.5Fe alloy with 60 % cold deformation is the highest after aging, and the maximum 270.1 HV hardness is obtained after aging at 500 °C for 1 h, while the maximum 22.3 % IACS conductivity is obtained after aging at 450 °C for 8 h. The maximum hardness of the alloy with 0 % deformation after aging is 193.5 HV. Fig. 2(e) and (f) show hardness and conductivity variations with aging time for the 60 % deformed Cu-1.5Ti-0.5Fe alloy. The peak hardness is 256.9 HV, 262.5 HV, 270.1 HV and 254.4 HV during the aging process of 400 °C, 450 °C, 500 °C, and 550 °C, respectively in Fig. 2(e).

The peak hardness gradually increases with aging temperature, but at higher aging temperature of 550 °C, the peak hardness decreases because compared with precipitation strengthening, the grain growth at this high temperature plays a dominant role. The peak hardness of the alloy aged at 400 °C, 450 °C, 500 °C and 550 °C corresponds to the 18.4 % IACS, 19.6 % IACS, 18.1 % IACS and 15.5 % IACS conductivity in Fig. 2(f). Fig. 2(g) shows the engineering stress-strain curves of the Cu-1.5Ti-0.3Fe and Cu-1.5Ti-0.5Fe alloys at different aging states. The tensile strength of the Cu-1.5Ti-0.3Fe alloy aged at the 450 °C and 500 °C is 742.1 MPa and 715.7 MPa, respectively, and the tensile strength of the Cu-1.5Ti-0.5Fe alloy aged at 450 °C and 500 °C peak is 739.6 MPa and 711.8 MPa, respectively. Both alloys achieve maximum tensile strength at 450 °C aging conditions. Interestingly, Cu-1.5Ti-0.3Fe alloy not only has good tensile strength, but also large elongation.

Fig. 2(h) shows the hardness of the two alloys deformed to 60 % after aging at different temperatures. The hardness of Cu-1.5Ti-0.3Fe is higher than Cu-1.5Ti-0.5Fe when aged at 450 °C and 500 °C. This is also consistent with the tensile test results in Fig. 2(g). Fig. 2(i) shows the peak aging hardness and conductivity of Cu-1.5Ti-0.3Fe and Cu-1.5Ti-0.5Fe with 60 % deformation. The hardness and conductivity of the two alloys increased with aging temperature, showing a trend of first rising and then decreasing. Although the two alloys have the highest hardness at 500 °C aging, the alloys have higher conductivity and tensile strength at 450 °C aging with only a slight decrease in hardness. Thus, the optimal aging process parameters for the balance of mechanical properties and electrical conductivity of the two alloys were obtained: 60 % cold deformation, 450 °C aging temperature, and 240 min aging time. The hardness, tensile strength and conductivity of the Cu-1.5Ti-0.3Fe alloy is 269.3 HV, 742.1 MPa and 19.8 % IACS, respectively, while the hardness, tensile strength and conductivity of the Cu-1.5Ti-0.5Fe alloy is 262.5 HV, 739.6 MPa and 19.6 % IACS, respectively.

3.2. EBSD analysis

In the aging process, different components have different effects on the precipitation of the secondary phases, grain growth and texture evolution. To study the microstructure changes of the Cu–Ti–Fe alloy during aging, EBSD analysis was carried out using two alloys with different iron content. Fig. 3 shows the inverse pole figure (IPF) EBSD diagram and grain size of the Cu-1.5Ti-0.3Fe and Cu-1.5Ti-0.5Fe alloys. The alloys underwent 60 % deformation and were aged at 450 °C for 240 min and 480 min, respectively. After 240 min aging at 450 °C, the grains of the Cu-1.5Ti-0.3Fe alloy still show obvious deformed characteristics in Fig. 3(a), and the direction of grain elongation is parallel to the rolling direction. Due to the cold deformation effects, a small number of twins still exist in the aged alloy, and recrystallized grains are formed in the area where the grains are violently broken. The average grain size of the alloy is 98.7 μm, and there are 39 % grains larger than 100 μm. Fig. 3(b) shows the Cu-1.5Ti-0.3Fe alloy structure after 480 min of 450 °C aging. With longer aging time, the elongated grains can still be seen along the rolling direction, the number of twins in the alloy structure is further reduced, and the recrystallization grains have grown to varying degrees. At 480 min aging time the average grain size increased to 121 μm, while the proportion of grains smaller than 50 μm decreased from 46.8 % to 37.5 %, and the proportion of grains larger than 100 μm increased to 44.3 %. This shows that the long-term aging allows the recrystallized grains sufficient time for nucleation and growth, which is also confirmed by the trends of conductivity and hardness in the aging process.

Fig. 3(c) and (d) show the EBSD diagram and grain size of the Cu-1.5Ti-0.5Fe alloy after 450 °C aging of 240 min and 480 min. The aging structure of the alloy clearly shows deformation and elongation along the rolling direction, and there are more recrystallized grains in Fig. 3(c). The average grain size of the alloy was 37.6 μm, and the grain size greater than 100 μm accounted for 7.7 %. The structure after 480 min aging is shown in Fig. 3(d), and its microstructure shows similar characteristics to Fig. 3(c). The average grain size is 25 μm, and the grain size greater than 100 μm accounts for only 3 %. Compared with the Cu-1.5Ti-0.3Fe alloy, the grain size of Cu-1.5Ti-0.5Fe is greatly reduced after aging. In the peak aging state, the grain size is reduced to 62 % after increasing the iron content. This is because the addition of alloying elements reduces the migration rate of the grain interface, and the densely precipitated secondary phase will also have a pinning effect on the grain interface, hindering grain growth. Fe can delay the recrystallization process and inhibit the grain growth during aging at 450 °C, which has great potential in improving the high temperature mechanical properties and enhancing the alloy thermal stability.

The deformation work consumed in the cold deformation process of metals is stored in the grains as dislocations, defects, subgrain boundaries and other structures. During the aging process, the alloy is at a higher temperature and the internal energy is released, often accompanied by the movement, elimination and combination of dislocations. Therefore, characterizing the distribution of dislocations in the alloy is helpful for studying structural changes during aging. Fig. 4 shows the kernel area misorientation (KAM) diagram and orientation angle distribution of the Cu-1.5Ti-0.3Fe and Cu-1.5Ti-0.5Fe alloys with 60 % deformation at different aging states. The red part in the KAM diagram is the area with a high dislocation density, and both alloys have different number of dislocations. The average dislocation density ρ in the alloy can be calculated as in Ref. [37]:

$$\rho = 2\theta/\mu b \tag{1}$$

Here, ρ is the geometrically necessary dislocation density in m^{-2}, θ is the

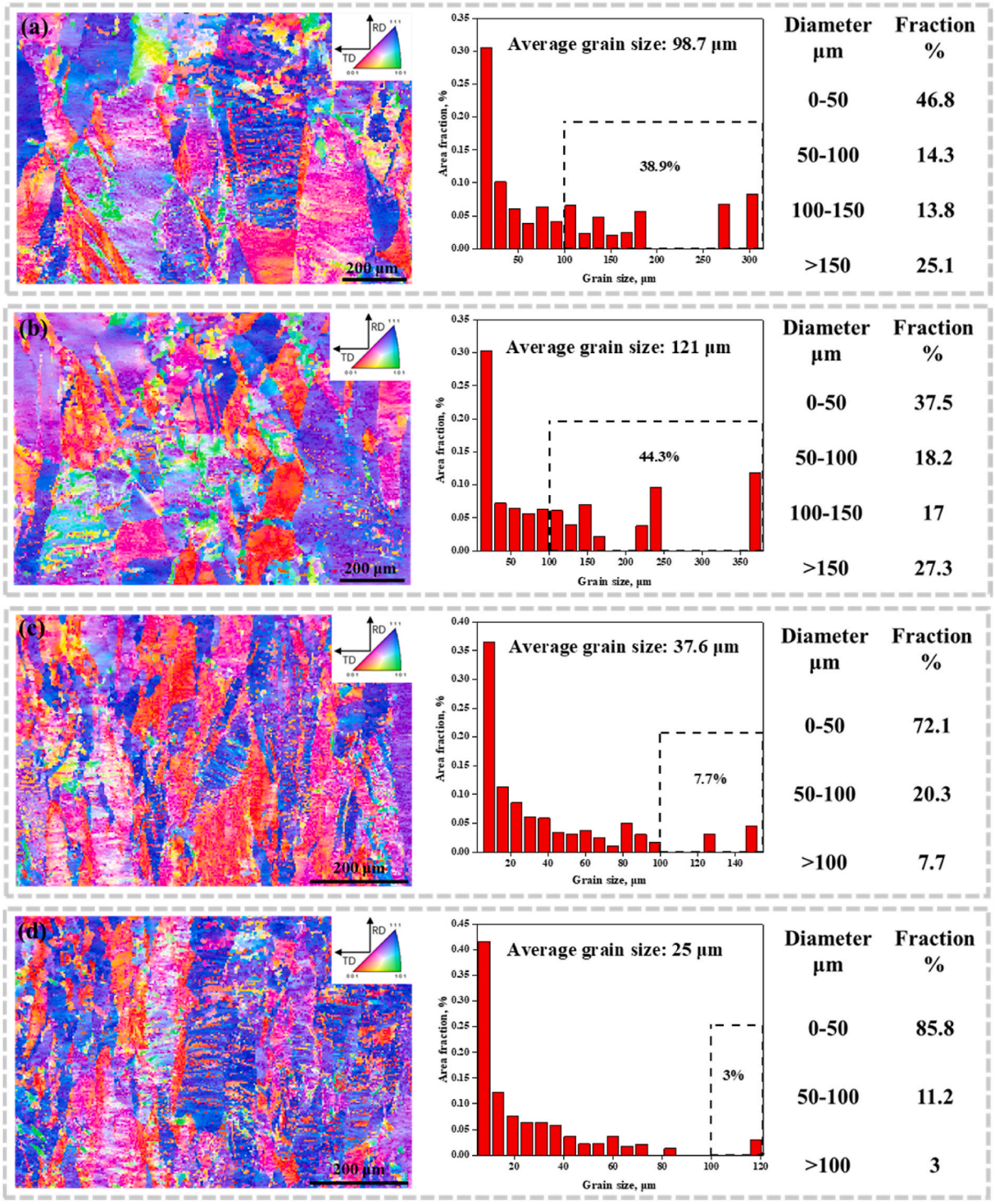

Fig. 3. EBSD diagram and grain size of the Cu-1.5Ti-0.3Fe and Cu-1.5Ti-0.5Fe alloys with 60 % deformation: (a) Cu-1.5Ti-0.3Fe alloy aged for 240 min at 450 °C; (b) Cu-1.5Ti-0.3Fe alloy aged for 480 min at 450 °C; (c) Cu-1.5Ti-0.5Fe alloy aged for 240 min at 450 °C; (d) Cu-1.5Ti-0.5Fe alloy aged for 480 min at 450 °C.

mean local orientation difference in radians, μ is the EBSD scanning step size in μm, and b is the Burgers vector of the alloy (0.255 nm). It can be seen from Fig. 4(a) and (b) that the average dislocation density of the Cu-1.5Ti-0.3Fe alloy aged at 450 °C for 240 min and 480 min is $\rho = 6.77 \times 10^{13}$ m^{-2} and $\rho = 6.53 \times 10^{13}$ m^{-2}, respectively. The average dislocation density of the Cu-1.5Ti-0.5Fe alloy aged at 450 °C for 240 min and 480 min is $\rho = 1.15 \times 10^{14}$ m^{-2} and $\rho = 1.12 \times 10^{14}$ m^{-2} in Fig. 4(c) and (d), respectively.

The dislocation density of Cu-1.5Ti-0.3Fe and Cu-1.5Ti-0.5Fe alloys decreases to varying degrees with aging time. This indicates that the dislocation-related energy storage structure inside the alloy releases distortion energy during aging, which further promotes the formation of recrystallized grains. A horizontal comparison of the KAM plots in Fig. 4 (a–c) and (b, d) shows that compared with Cu-1.5Ti-0.3Fe, the dislocation density of the Cu-1.5Ti-0.5Fe alloy is significantly higher for the same aging conditions. This further shows that increasing the Fe content can inhibit the dynamic recovery and recrystallization during aging, and the release of internal distortion energy is reduced, thereby retaining the

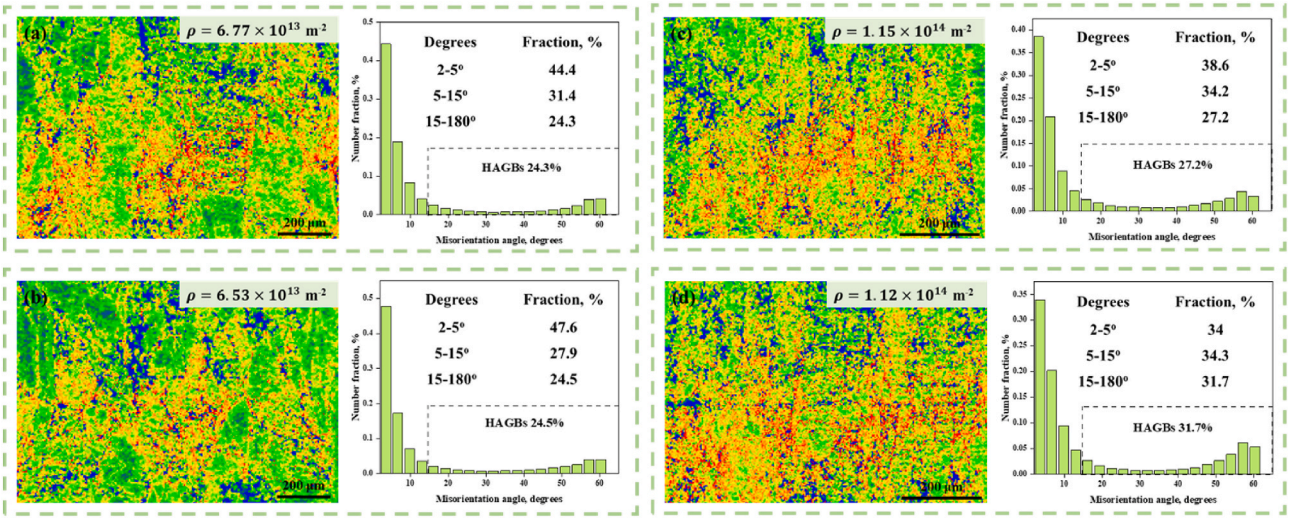

Fig. 4. Kernel average misorientation diagram and orientation angle distribution of the Cu-1.5Ti-0.3Fe and Cu-1.5Ti-0.5Fe alloys with 60 % deformation: (a) Cu-1.5Ti-0.3Fe alloy aged for 240 min at 450 °C; (b) Cu-1.5Ti-0.3Fe alloy aged for 480 min at 450 °C; (c) Cu-1.5Ti-0.5Fe alloy aged for 240 min at 450 °C; (d) Cu-1.5Ti-0.5Fe alloy aged for 480 min at 450 °C.

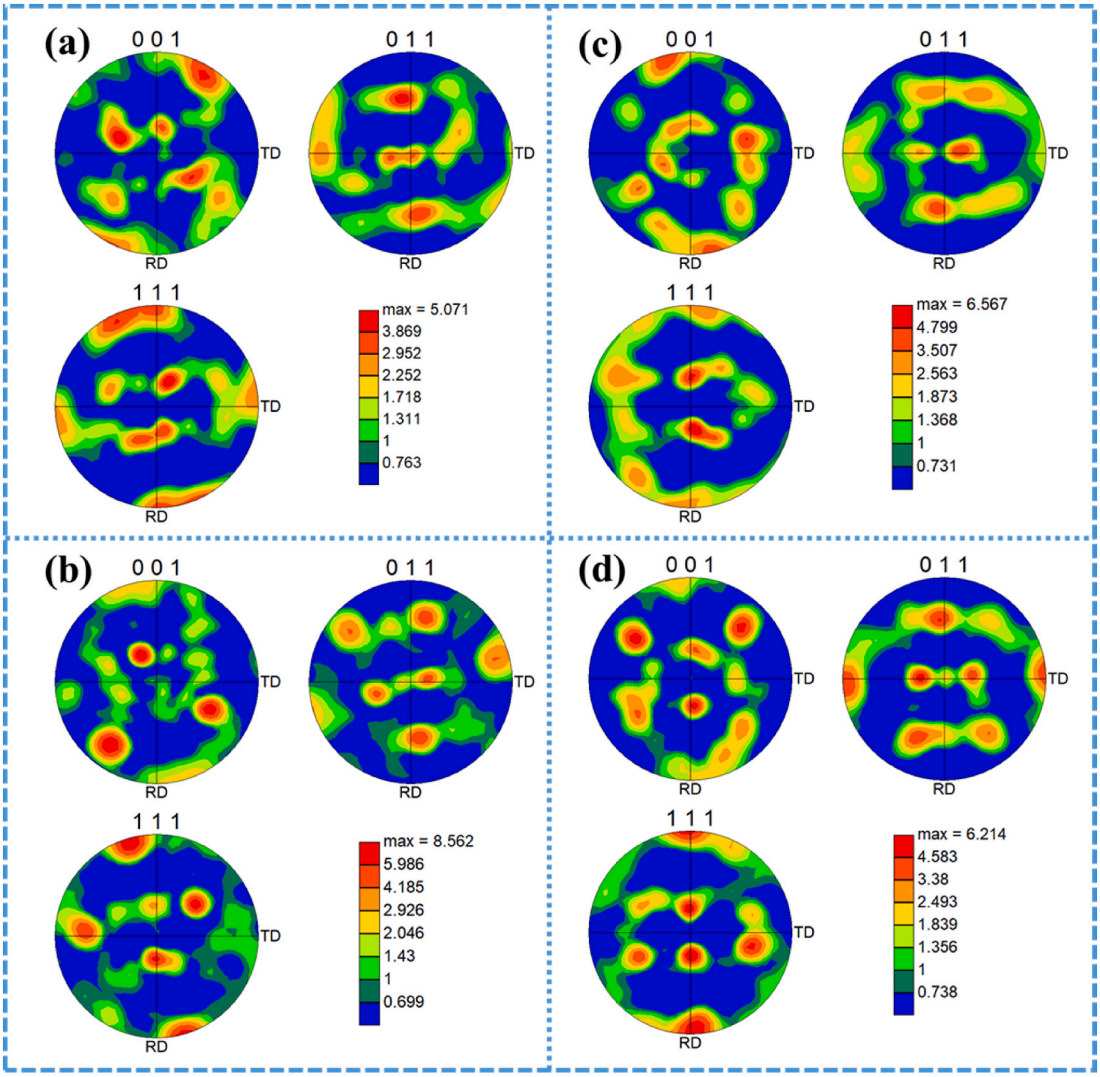

Fig. 5. Pole figures of the Cu-1.5Ti-0.3Fe and Cu-1.5Ti-0.5Fe alloys with 60 % deformation: (a) Cu-1.5Ti-0.3Fe alloy aged for 240 min at 450 °C; (b) Cu-1.5Ti-0.3Fe alloy aged for 480 min at 450 °C; (c) Cu-1.5Ti-0.5Fe alloy aged for 240 min at 450 °C; (d) Cu-1.5Ti-0.5Fe alloy aged for 480 min at 450 °C.

high dislocation density. It can be seen from the orientation angle distribution in Fig. 4(a) and (b) that the large angle grain boundaries of the Cu-1.5Ti-0.3Fe alloy aged at 450 °C for 240 min and 480 min are 24.3 % and 24.5 %, respectively. The orientation angle distribution in Fig. 4(c) and (d) shows that Cu-1.5Ti-0.5Fe alloy has 27.2 % and 31.7 % large angle grain boundaries when aged at 450 °C for 240 min and 480 min, respectively.

The proportion of large angle grain boundaries increased with aging time. This is because the small angle grain boundaries form the recrystallization core through the merger and migration mechanisms. The grain boundaries of the crystal nuclei grow to areas with high dislocation and large distortion energy, forming large angle grain boundaries during aging. Compared with Cu-1.5Ti-0.3Fe, the proportion of high angle grain boundaries in the Cu-1.5Ti-0.5Fe alloy is relatively high. This is because iron inhibits recrystallized grain growth, which gives regions with high dislocation density and high distortion energy enough time to form more nuclei, and eventually more and finer large-angle grains.

At larger deformation due to rolling, the grains inside the alloy will be broken and rearranged, so that they show a preferred orientation in a certain direction and form a deformation texture. In the aging process, due to the recrystallization effects, the grain will change, sometimes still showing a preferred orientation in a certain direction, forming a recrystallization texture. Therefore, the texture evolution can also reflect the organizational changes of the alloy aging process to a certain extent.

Fig. 5 shows the pole figures of 60 % deformed Cu-1.5Ti-0.3Fe and Cu-1.5Ti-0.5Fe alloys aged at 450 °C for 240 min and 480 min. Compared with the standard pole figures, the Cu-1.5Ti-0.3Fe shows strong characteristics of the {110}<112> Brass and {123}<634> S texture in Fig. 5(a) and (b). In Fig. 5(c) and (d) the texture of Cu-1.5Ti-0.5Fe after 240 min aging at 450 °C is mainly {110}<112> Brass texture and {123}<634> S texture, and the texture after 480 min aging is mainly {112}<111> Copper texture and {123}<634> S texture. After the aging time of the Cu-1.5Ti-0.3Fe alloy is extended from 240 min to 480 min, its maximum texture strength increases from 5.071 to 8.562. However, after the aging time of the Cu-1.5Ti-0.5Fe alloy is extended, the maximum texture strength does not change much, which may be caused by the increase of Fe content inhibiting the growth of recrystallized grains and the slow microstructure change.

Fig. 6 shows the texture content and distribution of the Cu-1.5Ti-0.3Fe and Cu-1.5Ti-0.5Fe alloys with 60 % deformation. Let's consider the Cu-1.5Ti-0.3Fe alloy in Fig. 6(a) as an example to study the texture evolution due to the aging process. After the 450 °C 240 min aging, the volume proportions of Cube, Goss, Brass, Copper and S texture were 4.49 %, 7.68 %, 31.4 %, 11.1 % and 24.3 %, respectively. The proportion of Cube and Goss texture increased, while the proportion of Brass, Copper and S texture decreased to varying degrees with longer aging time. The increase of the recrystallization Cube texture also indicates that the recrystallization degree of the Cu-1.5Ti-0.3Fe alloy is further improved after extending the aging time. In Fig. 6(b) the Cu-1.5Ti-0.5Fe alloy texture changes with aging time. The volume proportion of Cube, Goss and Brass texture decreases, while the volume proportion of Copper and S texture increases significantly, becoming the main alloy texture.

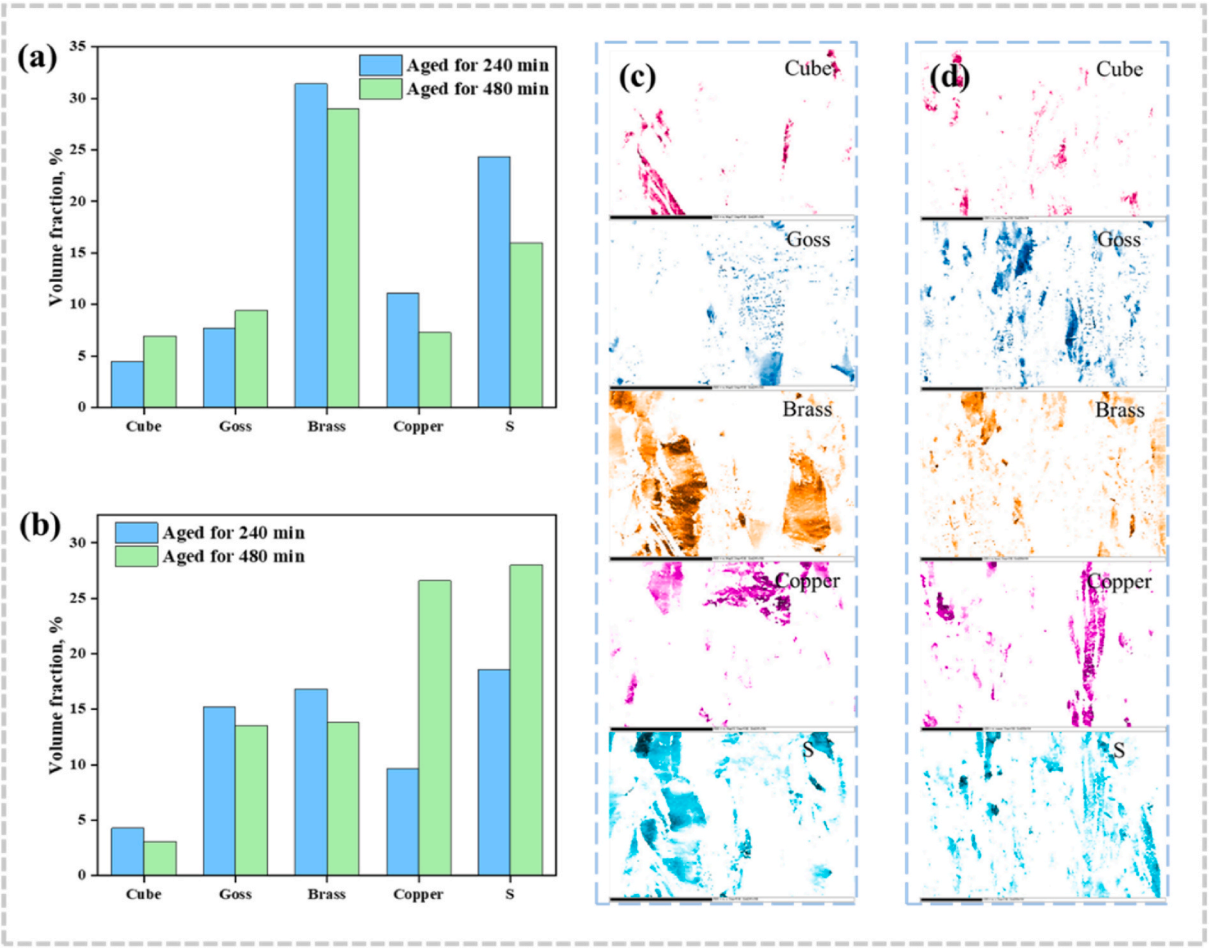

Fig. 6. Texture content a nd distribution of the Cu-1.5Ti-0.3Fe and Cu-1.5Ti-0.5Fe alloys with 60 % deformation at different aging states: (a) The texture of the Cu-1.5Ti-0.3Fe alloy aged at 450 °C for 240 min and 480 min; (b) The texture of the Cu-1.5Ti-0.5Fe alloy aged at 450 °C for 240 min and 480 min; (c) Texture distribution of the Cu-1.5Ti-0.3Fe alloy aged at 450 °C 240 min; (d) Texture distribution of the Cu-1.5Ti-0.5Fe alloy aged at 450 °C 240 min.

The difference in the main texture of the two alloys indicates that compared with the Cu-1.5Ti-0.3Fe alloy, the aged Cu-1.5Ti-0.5Fe alloy has a higher stacking fault energy. This is related to the internal distortion of the alloy after increasing the solute content, and at the same time, it also corresponds to the high dislocation density of the Cu-1.5Ti-0.5Fe alloy after aging.

3.3. TEM analysis

After the deformation and aging treatment of copper alloys, their strength will be greatly improved, which is inseparable from the changes in internal structure. Fig. 7 shows a TEM image of the aginged Cu-1.5Ti-0.3Fe alloy with 60 % deformation. There are obvious dislocation tangles and dislocation walls inside the alloy in Fig. 7(a). This is because the atoms inside the metal are misaligned under the action of external forces, forming dislocations during the deformation process. During the movement of the dislocations, the dislocations are intertwined to form this structure due to the hindrance of the precipitated phase. Fig. 7(b) shows multiple precipitated phases. The precipitated phases play the role of purifying the alloy matrix, nailing the dislocations, and improving the mechanical properties of the alloy. At the same time, due to the reduction of solid solution atoms between alloy matrixes, the lattice distortion of the matrix is further reduced, which is conducive to further improvement of copper alloys electrical conductivity.

In order to further explore the types of precipitated phases of the alloy, the Fourier transform was performed in the white box area in Fig. 7(c), and the diffraction spots are shown in Fig. 7(d). It is found after calibration that the nanoscale precipitated phase is Cu_4Ti, and the four crystal plane directions of the precipitated phase are $(200)_{Cu4Ti}$, $(113)_{Cu4Ti}$, $(013)_{Cu4Ti}$ and $(\bar{1}13)_{Cu4Ti}$ in Fig. 7(d). It was determined by inverse fast Fourier transform (IFFT) conversion of the diffraction spots in Fig. 7(d), that the crystal plane spacing of $(113)_{Cu4Ti}$ was 0.3053 nm and that of $(\bar{1}13)_{Cu4Ti}$ was 0.248 nm. In the IFFT diagram of Fig. 7(e and f) there are misaligned atoms and dislocations.

Fig. 8 shows a TEM image of the aged Cu-1.5Ti-0.5Fe alloy with 60 % deformation. In Fig. 8(a) there are obvious dislocation tangles and dislocation walls inside the alloy, and the dislocation density is significantly higher than Cu-1.5Ti-0.3Fe, which is consistent with the EBSD results. Two different types of precipitated phases can be observed from the HRTEM in Fig. 8(b). In order to explore the type of precipitated phase, the diffraction spot in Fig. 8(d) was obtained by performing the Fourier transform of the boxed region in Fig. 8(c). After calibration, the precipitated phase was determined as Cu_4Ti, and the four crystal plane directions of $(\bar{1}13)_{Cu4Ti}$, $(\bar{1}03)_{Cu4Ti}$, $(\bar{1}\bar{1}3)_{Cu4Ti}$ and $(0\bar{2}0)_{Cu4Ti}$ were obtained. By IFFT conversion of the diffraction spots in Fig. 8(d), the crystal plane spacing of $(0\bar{2}0)_{Cu4Ti}$ was determined to be 0.2133 nm, and the crystal plane spacing of $(\bar{1}13)_{Cu4Ti}$ was determined to be 0.2418 nm.

A short rod-like nano-precipitated phase can be seen in the white frame in Fig. 8(f), resulting in the diffraction spots shown in Fig. 8(g) by Fourier transform. Two sets of diffraction spots can be clearly seen in Fig. 8(g), and after calibration, the precipitated phases are determined to be Cu and Fe_2Ti. The orange part in Fig. 8(g) is calibrated as Cu, and there are three $(002)_{Cu}$, $(1\bar{1}1)_{Cu}$, and $(1\bar{1}\bar{1})_{Cu}$ crystal planes. The crystal plane spacing shown in Fig. 8(h and i) was obtained by inverse Fourier transform of the diffraction spots, and the crystal plane spacing of $(002)_{Cu}$ was determined to be 0.1821 nm, while the crystal plane spacing of $(1\bar{1}1)_{Cu}$ was 0.2099 nm. The blue part in Fig. 8(g) is calibrated as Fe_2Ti, and there are three crystal plane orientations: $(\bar{2}1\bar{1})_{Fe2Ti}$, $(\bar{1}21)_{Fe2Ti}$ and $(112)_{Fe2Ti}$. The facet spacing shown in Fig. 8(j and k) was obtained by performing the inverse Fourier transform of the diffraction spots, and the crystal plane spacing of $(\bar{2}1\bar{1})_{Fe2Ti}$ was determined to be 0.2369 nm, while the $(112)_{Fe2Ti}$ crystal plane spacing was 0.2049 nm. Fig. 8(l) is the atomic model of Fe_2Ti, which can intuitively demonstrate the stacking of Fe atoms and Ti atoms. It is found that in the aging process, the supersaturated Ti and Fe atoms in the Cu–Ti–Fe alloy

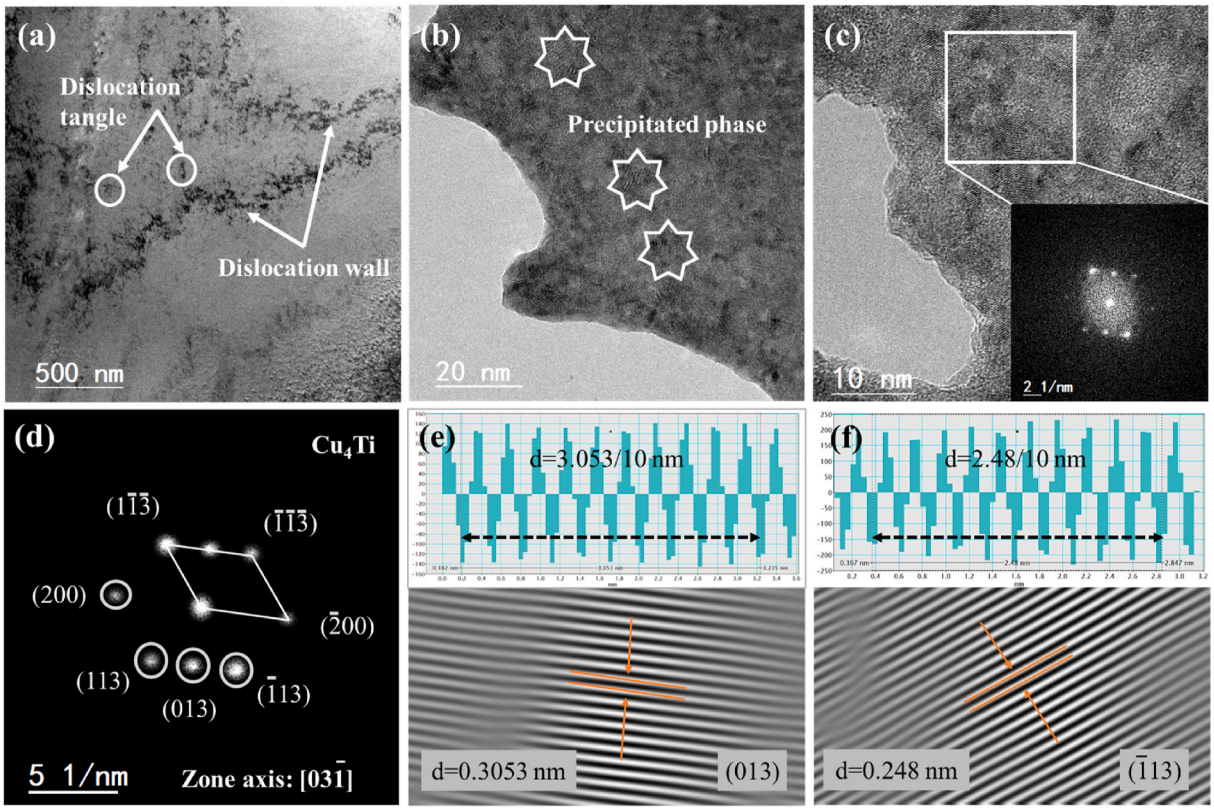

Fig. 7. TEM microstructure analysis of peak aging of the Cu-1.5Ti-0.3Fe alloy with 60 % deformation: (a) Brightfield image; (b, c) HRTEM microstructure of Cu_4Ti; (d) FFT diagram of Cu_4Ti (e, f) IFFT diagrams of Cu_4Ti.

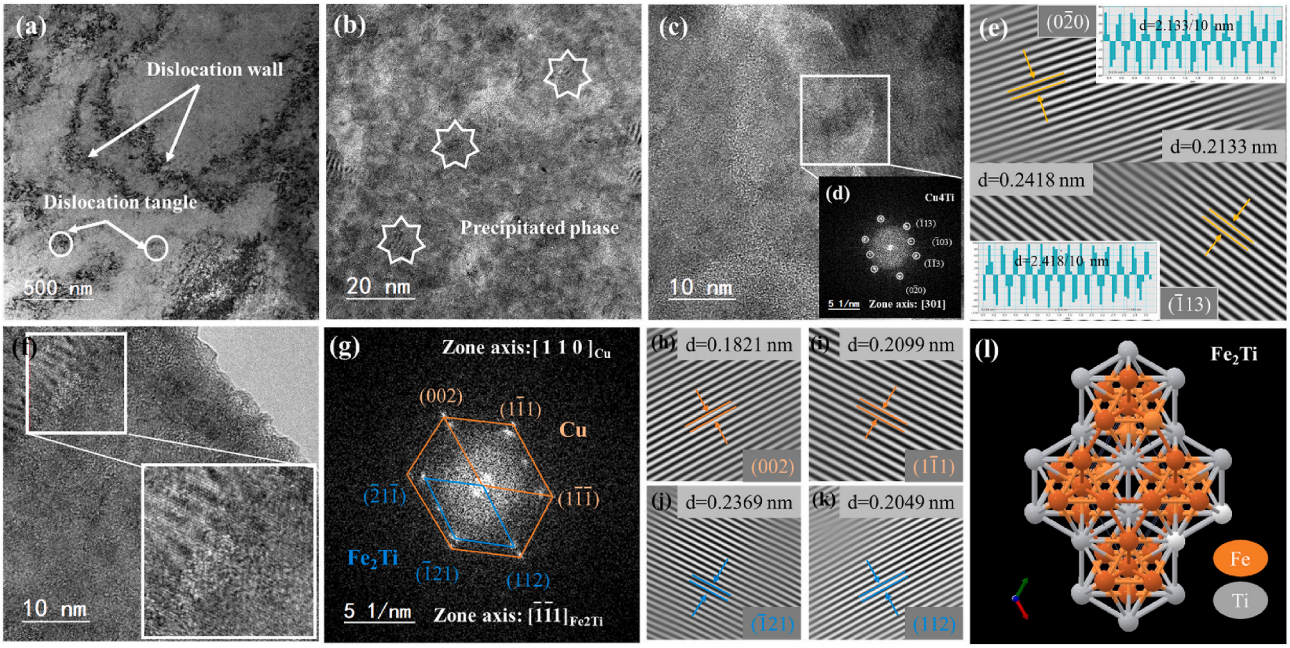

Fig. 8. TEM microstructure analysis of aged Cu-1.5Ti-0.5Fe alloy with 60 % deformation: (a) Brightfield image; (b, c) HRTEM microstructure of alloys; (d) FFT diagram of Cu_4Ti; (e) IFFT diagram of Cu_4Ti; (f) HETEM microstructure of the alloy; (g) FFT diagram of Cu and Fe_2Ti; (h, i) IFFT diagram of Cu; (j, k) IFFT diagram of Fe_2Ti; (l) Atomic stacking model of Fe_2Ti.

precipitated from the matrix in the form of precipitated phases, improving the alloy strength and electrical conductivity.

The main precipitated phases in Cu–Ti–Fe alloys are nanoscale Cu_4Ti and Fe_2Ti, but when the content of Fe is low, the precipitated phase is mainly Cu_4Ti. This is because lower Fe content can be completely dissolved in the copper matrix at room temperature, as it plays more of a solid solution strengthening role, and it is difficult to combine with other elements to form a precipitated phase. After further increasing the iron content, iron atoms that cannot be dissolved in the matrix will combine with titanium atoms to form a Fe_2Ti precipitated phase. Due to the consumption of titanium, this will reduce the precipitation of the Cu_4Ti phase. Due to the different strengthening effects of the two precipitated relative alloys, different precipitated phase content changes the alloy properties.

4. Discussion

4.1. Strengthening of copper alloys

In order to improve the strength of copper alloys and obtain excellent comprehensive properties, a variety of approaches are often used. In this experiment, trace amounts of Ti and Fe were added to the Cu matrix as solute elements, which were uniformly distributed in the matrix by solution treatment. Due to the difference in the atomic radii of the three metals, the crystal lattice causes distortion under the action of internal stress and improves the strength of the alloy. After that, the grains are broken during cold deformation of 60 %, and a large number of dislocation cells and walls are introduced, which further increases the strengthening effect. Finally, in the aging process, under the comprehensive action of the precipitation and recrystallization of the secondary phase, the alloy strength is further improved. These are the main strengthening mechanisms of copper alloys: grain boundary, solution, deformation, and precipitation strengthening. In order to evaluate the contribution of different strengthening mechanisms to the strength of Cu-1.5Ti-0.3Fe alloy, the combined yield strength of the alloy σ is separated into:

$$\sigma = \sigma_0 + \sigma_{GB} + \sigma_{ss} + \sigma_{ds} + \sigma_p \quad (2)$$

Here, the lattice frictional stress of the copper matrix σ_0 is 60 MPa [38]. σ_{GB}, σ_{ss}, σ_{ds} and σ_p correspond to the strength contributions due to grain boundary, solid solution, deformation, and precipitation strengthening, respectively.

The contribution of grain boundary strengthening can be described by the Hall-Petch formula [39,40]:

$$\sigma_{GB} = K_y d^{-1/2} \quad (3)$$

Here, d is the average grain size, 1/1/2024which is 98.7 μm in Fig. 3(a), and the Hall-Petch coefficient K_y is 150 MPa $\mu m^{1/2}$. Therefore, the grain boundary strengthening mechanism contributed 15.1 MPa to the Cu-1.5Ti-0.3Fe alloy strength.

σ_{ss} is the improvement of the alloy strength by the solid solution strengthening mechanism, which is closely related to the radius difference between the solute and matrix atoms, and is expressed as in Ref. [41]:

$$\sigma_{SS} = G\left(|\delta| + \frac{1}{20}\right)|\eta|^{\frac{3}{2}}\sqrt{\frac{x_a}{3}} \quad (4)$$

Here, $G = 46$ GPa is the shear modulus of the copper alloy. δ is a lattice change factor caused by solute elements, which is 0.1105. $\eta = 0.3171$ is a factor that describes the change in shear modulus. x_a is the percentage of solute atoms in the solid solution, which can be converted from the mass percentage to obtain $x_a = 1.98\% + 0.32\% = 2.3\%$. Therefore, the strength contribution of the solution strengthening mechanism to the Cu-1.5Ti-0.3Fe alloy is 115.4 MPa.

After 60 % cold deformation, a large number of deformation bands, dislocation cells and other morphology features are introduced into the copper alloy, and the strength of the alloy is greatly improved by their joint action as in Ref. [42]:

$$\sigma_{ds} = M\alpha G b\sqrt{\rho} \quad (5)$$

Here, $M = 3.06$ is the Taylor factor of the copper alloy. $\alpha = 0.3$ is a geometric constant. $G = 46$ GPa is the shear modulus of copper alloys. B is the Burgers vector of the copper alloy (0.2556 nm). ρ is the dislocation density, as in Fig. 4(a), $\rho = 6.77 \times 10^{-13}\, m^{-2}$. Therefore, the

deformation strengthening mechanism contributed 88.8 MPa to the strength of the Cu-1.5Ti-0.3Fe alloy. Finally, one can obtain the improvement of the alloy strength by the precipitation strengthening mechanism: $\sigma_p = \sigma - \sigma_0 - \sigma_{GB} - \sigma_{ss} - \sigma_{ds} = 462.8\ MPa$. In the same way, the contribution of different strengthening methods to the strength of Cu-1.5Ti-0.5Fe alloy is calculated, as shown in Fig. 9(a).

Fig. 9(a) shows the strength contribution of different strengthening mechanisms to the two alloys. As can be seen from the figure, with the increase of the content of Fe atoms in solute atoms, the contribution of grain boundary strengthening, solution strengthening and deformation strengthening mechanisms to the strength of the alloy increases significantly. This is because after the addition of solute atoms, the resistance of dislocation motion becomes larger, and the cold deformation makes more dislocations retain inside the alloy, which enhances the effect of solution strengthening and deformation strengthening. Finer grains result in more grain boundaries inside the alloy, which facilitates grain boundary strengthening.

It can also be seen from Fig. 9(a) that precipitation strengthening is the main strengthening mechanism of copper alloys, which is an important reason for the high strength of Cu–Ti–Fe alloys. Fig. 9(b and c) show the tensile fracture morphology of the two aged alloys, where the fracture surfaces of both alloys have a large number of dimples, manifesting plastic fracture. Among them, the dimples of the Cu-1.5Ti-0.3Fe alloy are larger and deeper, while the dimples of Cu-1.5Ti-0.5Fe alloy are relatively small. This shows that the Cu-1.5Ti-0.3Fe alloy has better plasticity after aging, which is also consistent with the stress-strain curves in Fig. 2(g).

4.2. Transition analysis of the precipitated phase

After solution treatment, excessive Ti and Fe atoms distort the crystal lattice of the copper matrix to form a supersaturated solid solution, and these internal distortion stresses will hinder the movement of electrons and reduce the conductivity of the Cu–Ti–Fe alloy. With the advancement of the aging process, Ti and Fe atoms in the solid solution are continuously precipitated to form dispersed fine precipitated phase particles. The strength of the alloy is greatly improved during this process. The electrical conductivity will also increase with the continuous purification of the matrix. The alloy electrical conductivity and the conversion variable of the precipitated phase are proportional. Therefore, to a certain extent, the change in conductivity can reflect the degree of transformation of the precipitated phase [43]. Therefore, the amount of precipitation phase conversion variable (PPCV) during alloy aging can be expressed by Ref. [44]:

$$f = V/V_c \tag{6}$$

Here, V is the precipitated phase volume precipitated under certain aging conditions, and V_c is the equilibrium volume of the precipitated phase after aging completion. The resistivity R of an alloy is expressed using the Machisen-Fuleminger rule:

$$R = R_0 + \alpha R_1 \tag{7}$$

Here, R is the measured electrical resistivity of the alloy, R_0 is the matrix resistivity, α is the mass ratio of solute atoms, and R_1 represents the resistivity of the alloy when the solute atoms content is 1 %. Since there is a relationship between resistivity R and conductivity γ, and the precipitated phase is continuously precipitated during aging, the relationship between conductivity and PPCV is expressed as:

$$\gamma = \gamma_0 + Af \tag{8}$$

Here, γ is the electrical conductivity of the alloy after aging, γ_0 is the conductivity of the alloy in the cold-rolled state, and A is the conductivity coefficient. Let's consider an example of Cu-1.5Ti-0.3Fe 450 °C aging after 60 % cold rolling. From the measured conductivity of Cu-1.5Ti-0.3Fe alloy in different aging states in Table 2, the following formula can be obtained:

$$\gamma = 7.79 + 13.85 \times f \tag{9}$$

Therefore, according to the conductivity of the alloys at different aging times, the precipitated phase conversion variable of the two alloys in different aging states can be calculated, as shown in Table 2.

It can be seen from Table 2 that with the continuous precipitation of solute atoms during the aging process, the volume fraction of the precipitated phase continues to increase. The lattice distortion of the alloy matrix is weakened, the scattering effect on electrons is reduced by the purified matrix, and the conductivity of the alloy is significantly increased. Compared with the conductivity of the cold-rolled state, the conductivity at the end of aging is nearly three times higher, and the increase is obvious.

In the aging process of Cu-1.5Ti-0.3Fe alloy, the relationship between aging time t and secondary phase change rate f can be expressed by the empirical equation of precipitation dynamics [32,45]:

$$f = 1 - \exp(-mt^n) \tag{10}$$

(a)

Strengthening mechanism	Strength, MPa	
	Cu-1.5Ti-0.3Fe	Cu-1.5Ti-0.5Fe
σ_0	60	60
σ_{GB}	15.1	24.5
σ_{ss}	115.4	122.3
σ_{ds}	88.8	115.7
σ_p	462.8	417.1

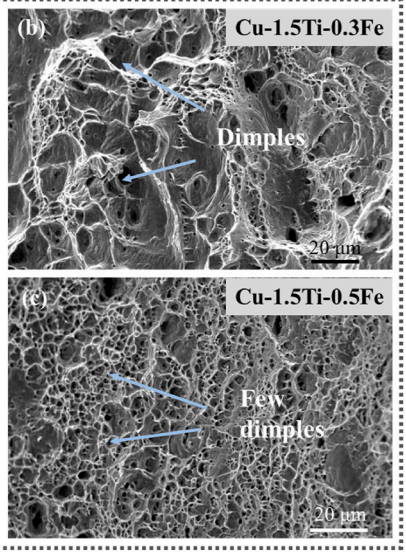

Fig. 9. (a) Strength contribution of different reinforcement mechanisms; (b, c) Tensile fracture morphology of 60 % deformed aged Cu-1.5Ti-0.3Fe and Cu-1.5Ti-0.5Fe alloys.

Table 2
Conductivity (measured value) and PPCV (calculated value) of Cu-1.5Ti-0.3Fe and Cu-1.5Ti-0.5Fe at 450 °C aging.

Alloy	Aging time, h	0	0.25	0.5	1	2	4	6	8
Cu-1.5Ti-0.3Fe	Conductivity, % IACS	7.79	10.49	14.39	15.86	17.75	19.79	20.76	21.64
Cu-1.5Ti-0.3Fe	PPCV, %	0	19.53	47.68	58.31	71.89	86.68	93.63	100
Cu-1.5Ti-0.5Fe	Conductivity, % IACS	8.29	11.06	13.78	16.13	17.95	19.65	21.13	22.30
Cu-1.5Ti-0.5Fe	PPCV, %	0	19.77	39.19	55.96	68.95	81.08	91.65	100

Here, m and n are constants, m is related to factors such as grain size, temperature and initial phase composition. After deforming the formula, take the logarithm of base 10 on both sides, and the formula can be expressed as:

$$\lg\left(\ln\frac{1}{1-f}\right)=n\lg(t)+\lg(m) \tag{11}$$

Fig. 10(a) was constructed using the calculated data in Table 2, which have a linear relationship $y = 0.7235x - 0.1041$. Here, the constant n is the slope of the fitted line $n = 0.72$. $\lg(m)$ is the intercept of the fitted line, and the result is $m = 0.79$.

By using the obtained constants in equation (10), the phase transition kinetic equation of the Cu-1.5Ti-0.3Fe alloy with 60 % deformation aged at 450 °C can be written as:

$$f_{450°C}=1-\exp\left(-0.79t^{0.72}\right) \tag{12}$$

By using the phase transition kinetic equation (12) with equation (8), the conductivity equation of Cu-1.5Ti-0.3Fe alloy with 60 % deformation aged at 450 °C can be obtained:

$$\gamma_{450°C}=7.79+13.85\times\left[1-\exp\left(-0.79t^{0.72}\right)\right] \tag{13}$$

Similarly, from Fig. 10(c), it can be seen that during the aging process of Cu-1.5Ti-0.5Fe alloy 450 °C, n = 0.71, b = 0.71, the phase transition dynamics equation and the conductivity equation are shown in equations (14) and (15):

$$f_{450°C}=1-\exp\left(-0.71t^{0.71}\right) \tag{14}$$

$$\gamma_{450°C}=8.29+14.01\times\left[1-\exp\left(-0.71t^{0.71}\right)\right] \tag{15}$$

In order to verify the accuracy of the conductivity equation of Cu-1.5Ti-0.3Fe and Cu-1.5Ti-0.5Fe alloys at an aging temperature of 450 °C, the calculated values of conductivity can be obtained by bringing the aging time into equations (13) and (15), respectively. Table 3 compares the test and calculated values.

As can be seen from Table 3, the measured and calculated values of the alloy conductivity are basically close. This shows that the conductivity equation of the alloy can accurately reflect the actual conductivity of Cu-1.5Ti-0.3Fe and Cu-1.5Ti-0.5Fe alloys with 60 % cold-rolled amount at 450 °C.

In order to visualize the transition of the precipitated phase of the alloy, the phase transition kinetic S-curve of the alloy during aging at 450 °C is shown in Fig. 10(b–d). At the initial stage of phase transition,

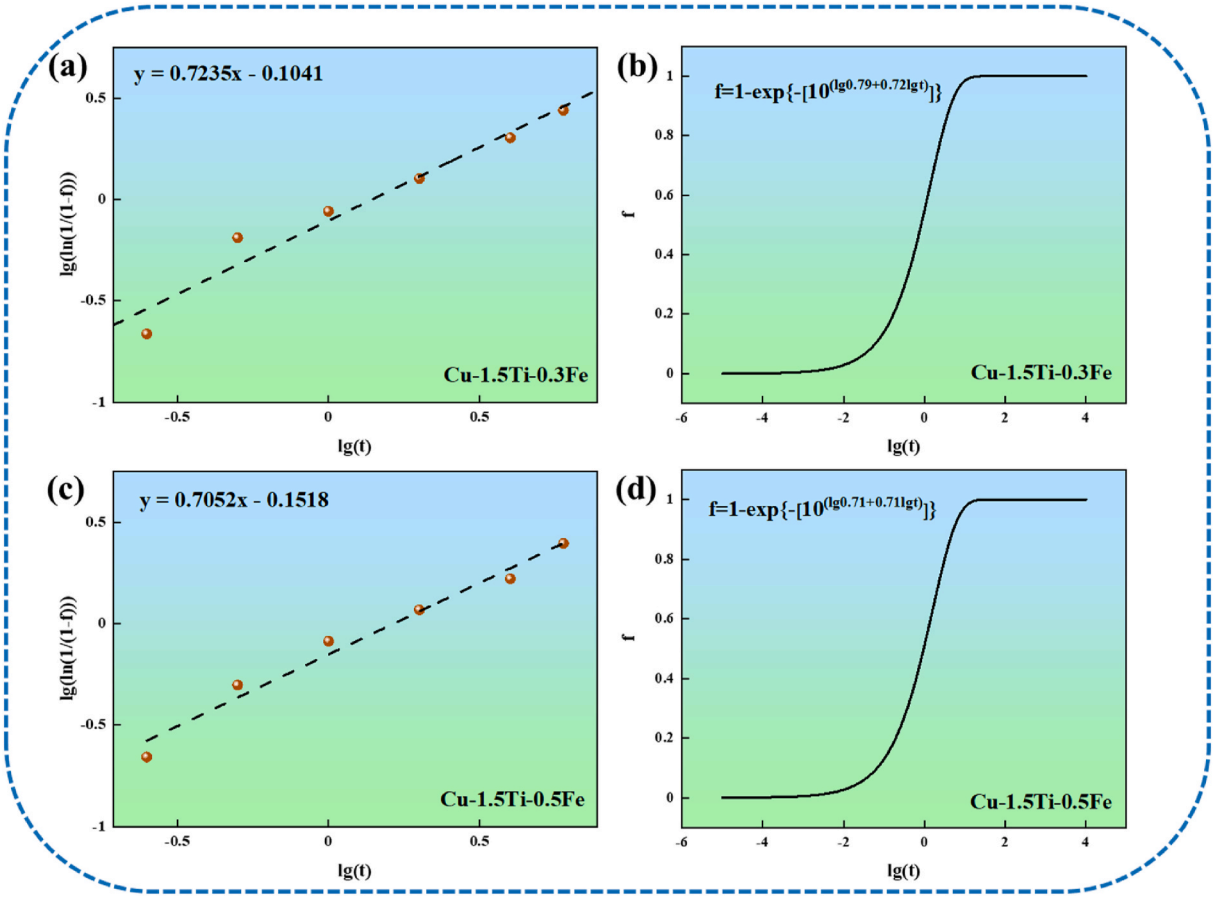

Fig. 10. Alloys with 60 % cold deformation are aged at 450 °C: (a,c) linear fitting plot of precipitation phase conversion variable and aging time; (b,d) Phase transition dynamics S-curve for ageing processes.

Table 3
Measured and calculated values of electrical conductivity.

Alloy	Aging time, h	0	0.25	0.5	1	2	4	6	8
Cu-1.5Ti-0.3Fe	Measurement, % IACS	7.79	10.49	14.39	15.86	17.75	19.79	20.76	21.64
Cu-1.5Ti-0.3Fe	Calculation, % IACS	7.79	11.29	13.07	15.35	17.87	20.02	20.85	21.23
Cu-1.5Ti-0.5Fe	Measurement, % IACS	8.29	11.06	13.78	16.13	17.95	19.65	21.13	22.30
Cu-1.5Ti-0.5Fe	Calculation, % IACS	8.29	11.56	13.22	15.41	17.91	20.20	21.19	21.67

the precipitation phase transformation rate of the alloy is low, and with the longer aging time, the transformation rate of the precipitated phase increases rapidly, while at the later aging stage, the transformation of the precipitated phase tends to be slower again. When *f* is less than 0.2, that is, the stage where the precipitation phase conversion variable is less than 20 %, the speed of alloy precipitation phase conversion increases the most. This also means that the alloy's conductivity increases at the fastest rate at the beginning of aging, which is also confirmed by the increasing trend of conductivity in Fig. 2(c).

It can be seen from the strengthening contribution equations (2)–(5) that precipitation strengthening is the most important strengthening method in the Cu–Ti–Fe alloy aging process. For precipitation-strengthened copper alloys, the content of solute elements in the copper matrix has a huge impact on the conductivity of the alloy. Due to the scattering of solute atoms, too many solute atoms will hinder the movement of electrons, resulting in increased resistivity. Therefore, the phase transition kinetic equation and the conductivity equation show that with the continuous precipitation of the precipitated phase in the supersaturated solid solution, not only it has a huge impact on the strength of the alloy, but also greatly improves the conductivity, while the precipitated phase is also an important factor affecting the alloy conductivity. By regulating the precipitated phase in the aging process and strictly controlling the aging parameters, the precipitation strengthening effect and the dynamic softening effect are balanced to obtain Cu–Ti–Fe alloy with excellent comprehensive performance.

5. Conclusions

(1) Cold deformation of 60 %, aging at 450 °C for 240 min, can optimize the hardness and conductivity of the Cu–Ti–Fe alloy. After treatment, Cu-1.5Ti-0.3Fe alloy hardness and electrical conductivity increased from 196.8 HV to 7.8 % IACS to 269.3 HV and 19.8 % IACS, with a tensile strength of 742.1 MPa.
(2) The main precipitated phase in the Cu-1.5Ti-0.3Fe and Cu-1.5Ti-0.5Fe alloys are Cu_4Ti, Cu_4Ti and Fe_2Ti phases, respectively. The Cu_4Ti and Fe_2Ti phases could purify the matrix and delays recrystallization, which effectively improving the strength of Cu–Ti–Fe alloys. In particular nanoscale Fe_2Ti phase strongly obstructs recrystallization and grain growth.
(3) Upon calculation, it was determined that the precipitation strengthening mechanism is the primary contributor to the high strength of the Cu–Ti–Fe alloy. Enhancing the concentration of solute atoms can lead to improved grain boundary strengthening, solution strengthening, and deformation strengthening.

CRediT authorship contribution statement

Gang'ao Xin: Conceptualization, Formal analysis, Methodology, Writing – original draft, Writing – review & editing. **Meng Zhou:** Project administration, Resources. **Ke Jing:** Resources, Supervision. **Haoyan Hu:** Resources, Software. **Zheng'ao Li:** Formal analysis. **Yi Zhang:** Funding acquisition, Resources, Writing – review & editing. **Qian Bai:** Investigation. **Caijiao Tian:** Methodology. **Baohong Tian:** Resources, Supervision. **Xu Li:** Investigation. **Alex A. Volinsky:** Writing – review & editing. **Jin Zou:** Formal analysis.

Declaration of competing interest

The authors declare that they have no known competing financial interests or personal relationships that could have appeared to influence the work reported in this paper.

Data availability

Data will be made available on request.

Acknowledgments

This work was supported by the National Natural Science Foundation of China (52071134), the Natural Science Foundation of Henan Province (232300420089), the Technology Innovation Center of Graphene Metrology and Standardization for State Market Regulation (AKYKF2309), the Program for Innovative Research Team at the University of the Henan Province (22IRTSTHN001), the China Postdoctoral Science Foundation (2023TQ0107), Key Research and Development Program of Jiangxi Province (20224BBE52002).

References

[1] K. Fukamachi, M. Kimura, Age-hardening structure and mechanism of Cu-3at%Ni-1.5 at%Si Corson alloy, Materials Science and Engineering a-Structural Materials Properties Microstructure and Processing 831 (2022), https://doi.org/10.1016/j.msea.2021.142220.
[2] J.P. Qu, S.P. Yue, W.S. Zhang, B.W. Dong, Y.J. Wang, J.C. Jie, T.M. Wang, T.J. Li, Optimization of microstructure and properties of as-cast various Si containing Cu-Cr-Zr alloy by experiments and first-principles calculation, Materials Science and Engineering a-Structural Materials Properties Microstructure and Processing 831 (2022), https://doi.org/10.1016/j.msea.2021.142353.
[3] K. Yang, Y. Wang, M. Guo, H. Wang, Y. Mo, X. Dong, H. Lou, Recent development of advanced precipitation-strengthened Cu alloys with high strength and conductivity: a review, Prog. Mater. Sci. 138 (2023), https://doi.org/10.1016/j.pmatsci.2023.101141.
[4] J. Yu, F. Zhao, H. Yang, J. Liu, J. Ma, Y. Fang, Progress in research on nanoprecipitates in high-strength conductive copper alloys: a review, J. Zhejiang Univ. - Sci. 24 (3) (2023) 206–225, https://doi.org/10.1631/jzus.A2200398.
[5] Y.-W. Hung, D.-P. Tran, C. Chen, Effect of Cu ion concentration on microstructures and mechanical properties of nanotwinned Cu foils fabricated by rotary electroplating, Nanomaterials 11 (8) (2021), https://doi.org/10.3390/nano11082135.
[6] Y.g. Wang, H.-y. Li, X.-y. Yuan, Y.-b. Jiang, Z.-a. Xiao, Z. Li, Review of copper and copper alloys as immune and antibacterial element, Trans. Nonferrous Metals Soc. China 32 (10) (2022) 3163–3181, https://doi.org/10.1016/s1003-6326(22)66011-4.
[7] T. Cao, S. Wang, G. Zhao, X. Wu, P.K. Liaw, J. Qiao, Evolution of microstructure and residual stress for a lead-frame Cu-2.13Fe-0.026 P (wt%) alloy, J. Alloys Compd. 965 (2023), https://doi.org/10.1016/j.jallcom.2023.171383.
[8] X. Zhang, Y. Zhang, B. Tian, K. Song, P. Liu, Y. Jia, X. Chen, J. An, Z. Zhao, Y. Liu, A.A. Volinsky, X. Li, T. Yin, Review of nano-phase effects in high strength and conductivity copper alloys, Nanotechnol. Rev. 8 (1) (2019) 383–395, https://doi.org/10.1515/ntrev-2019-0034.
[9] Q. Gong, J. Liu, F. Wu, H. Chen, W. Xie, H. Wang, B. Yang, Precipitation behavior and strengthening effects of the Cu-0.42Cr-0.16Co alloy during aging treatment, J. Alloys Compd. 936 (2023), https://doi.org/10.1016/j.jallcom.2022.168269.
[10] X. Huang, G. Xie, X. Liu, H. Fu, L. Shao, Z. Hao, The influence of precipitation transformation on Young's modulus and strengthening mechanism of a Cu-Be binary alloy, Materials Science and Engineering a-Structural Materials Properties Microstructure and Processing 772 (2020), https://doi.org/10.1016/j.msea.2019.138592.
[11] Y. Tu, X. Liu, W. Wang, W. Zhang, Q. Feng, Deformation-aging behavior and property evolution of Cu-Ti alloys prepared by accumulative roll bonding-deformation diffusion process, Materials Science and Engineering a-Structural Materials Properties Microstructure and Processing 855 (2022), https://doi.org/10.1016/j.msea.2022.143915.

[12] Y.-H. Yang, S.-Y. Li, Z.-S. Cui, Z. Li, Y.-P. Li, Q. Lei, Microstructure and properties of high-strength Cu-Ni-Si-(Ti) alloys, Rare Met. 40 (11) (2021) 3251–3260, https://doi.org/10.1007/s12598-020-01699-5.
[13] Z. Lai, K. Peng, B. Gao, Y. Mai, X. Jie, Achieving high strength and high electrical conductivity in Cu-Cr-Zr alloy by modifying shear banding during rolling, J. Alloys Compd. 958 (2023), https://doi.org/10.1016/j.jallcom.2023.170402.
[14] Y. Zhou, J. Yang, K. Song, S. Yang, Q. Zhu, X. Peng, Y. Liu, Y. Du, S. He, Effect of annealing temperature on dual-structure coexisting precipitates in Cu-2.18Fe-0.03P alloy and softening mechanism at high temperature, J. Mater. Sci. 57 (44) (2022) 20815–20832, https://doi.org/10.1007/s10853-022-07910-5.
[15] H. Zhang, Y. Jiang, J. Xie, Y. Li, L. Yue, Precipitation behavior, microstructure and properties of aged Cu-1.7 wt% Be alloy, J. Alloys Compd. 773 (2019) 1121–1130, https://doi.org/10.1016/j.jallcom.2018.09.296.
[16] J.C. Pang, Q.Q. Duan, S.D. Wu, S.X. Li, Z.F. Zhang, Fatigue strengths of Cu-Be alloy with high tensile strengths, Scripta Mater. 63 (11) (2010) 1085–1088, https://doi.org/10.1016/j.scriptamat.2010.08.009.
[17] S. Li, Z. Li, Z. Xiao, S. Li, L. Shen, Q. Dong, Microstructure and property of Cu-2.7Ti-0.15Mg-0.1Ce-0.1Zr alloy treated with a combined aging process, Materials Science and Engineering a-Structural Materials Properties Microstructure and Processing 650 (2016) 345–353, https://doi.org/10.1016/j.msea.2015.10.062.
[18] L. Huang, Z. Cui, X. Meng, X. Li, X. Sheng, Q. Lei, Effect of trace alloying elements on the stress relaxation properties of high strength Cu-Ti alloys, Materials Science and Engineering a-Structural Materials Properties Microstructure and Processing 846 (2022), https://doi.org/10.1016/j.msea.2022.143281.
[19] H. Jiao, J. Song, Separation of metallic Ti from Cu-Ti alloys through a simple and efficient electrochemical approach, Separ. Purif. Technol. 256 (2021), https://doi.org/10.1016/j.seppur.2020.117810.
[20] S. Semboshi, M. Ishikuro, S. Sato, K. Wagatsuma, T. Takasugi, Extraction of precipitates from age-hardenable Cu-Ti alloys, Mater. Char. 82 (2013) 23–31, https://doi.org/10.1016/j.matchar.2013.04.016.
[21] L. Huang, Z. Cui, X. Meng, X. Zhang, X. Zhang, X. Song, N. Tang, Z. Xiao, Q. Lei, Z. Li, Effects of microelements on the microstructure evolution and properties of ultrahigh strength Cu-Ti alloys, Materials Science and Engineering a-Structural Materials Properties Microstructure and Processing 823 (2021), https://doi.org/10.1016/j.msea.2021.141581.
[22] Z. Rdzawski, J. Stobrawa, W. Gluchowski, J. Konieczny, Thermomechanical processing of CuTi4 alloy, M. Eng. 42 (2010) 9–25.
[23] S. Nagarjuna, M. Srinivas, K. Balasubramanian, D.S. Sarma, On the variation of mechanical properties with solute content in Cu–Ti alloys, Mater. Sci. Eng., A 259 (1) (1999) 34–42, https://doi.org/10.1016/S0921-5093(98)00882-X.
[24] L. Huang, L. Peng, X. Mi, G. Zhao, G. Huang, H. Xie, W. Zhang, Relationship between microstructure and properties of high-strength Cu-Ti-Cr alloys during aging, J. Alloys Compd. 942 (2023), https://doi.org/10.1016/j.jallcom.2023.168865.
[25] T.K. Vaidyanathan, K. Mukherjee, Precipitation in Cu-Ti and Cu-Ti-Al alloys; discontinuous and localised precipitation, Mater. Sci. Eng. 24 (1) (1976) 143–152, https://doi.org/10.1016/0025-5416(76)90104-X.
[26] C. Li, X. Wang, B. Li, J. Shi, Y. Liu, P. Xiao, Effect of cold rolling and aging treatment on the microstructure and properties of Cu-3Ti-2Mg alloy, J. Alloys Compd. 818 (2020), https://doi.org/10.1016/j.jallcom.2019.152915.
[27] L. Huang, Z. Cui, X. Meng, X. Zhang, X. Zhang, X. Song, N. Tang, Z. Xiao, Q. Lei, Z. Li, Effects of microelements on the microstructure evolution and properties of ultrahigh strength Cu–Ti alloys, Mater. Sci. Eng., A 823 (2021) 141581, https://doi.org/10.1016/j.msea.2021.141581.
[28] L. Mineau, S. Hamar-Thibault, C.J.P.S.S. Allibert, Precipitation in Cu-rich CuFeTi Ternary Alloys — a Continuous Process? 137 (1993) 87–100.
[29] J.L. Murray, The Fe−Ti (Iron-Titanium) system, Bulletin of Alloy Phase Diagrams 2 (3) (1981) 320–334, https://doi.org/10.1007/BF02868286.
[30] S. Tang, Z. Xiao, Y. Ding, Y. Li, R. Wang, Y. Jia, S. Gong, Z. Li, Precipitation behavior and mechanical properties of a novel Cu–2Fe-0.5Ti alloy produced by thermos-mechanical treatment, Mater. Sci. Eng., A 882 (2023) 145453, https://doi.org/10.1016/j.msea.2023.145453.
[31] H. Yang, K. Li, Y. Bu, J. Wu, Y. Fang, L. Meng, J. Liu, H. Wang, Nanoprecipitates induced dislocation pinning and multiplication strategy for designing high strength, plasticity and conductivity Cu alloys, Scripta Mater. 195 (2021), https://doi.org/10.1016/j.scriptamat.2021.113741.
[32] H. Yang, Y. Bu, J. Wu, Y. Fang, J. Liu, L. Huang, H. Wang, High strength, high conductivity and good softening resistance Cu-Fe-Ti alloy, J. Alloys Compd. 925 (2022), https://doi.org/10.1016/j.jallcom.2022.166595.
[33] B. Rouxel, C. Cayron, J. Bornand, P. Sanders, R.E. Loge, Micro-addition of Fe in highly alloyed Cu-Ti alloys to improve both formability and strength, Mater. Des. 213 (2022), https://doi.org/10.1016/j.matdes.2021.110340.
[34] S. Tang, M. Zhou, Y. Zhang, D. Xu, Z. Zhang, X. Zheng, D. Li, X. Li, B. Tian, Y. Jia, Y. Liu, A.A. Volinsky, E.S. Marchenko, Improved microstructure, mechanical properties and electrical conductivity of the Cu-Ni-Sn-Ti-Cr alloy due to Ce micro-addition, Materials Science and Engineering a-Structural Materials Properties Microstructure and Processing 871 (2023), https://doi.org/10.1016/j.msea.2023.144910.
[35] M. Li, J. Liu, S. Yan, W. Yan, B. Shi, Effect of aging treatment on damping capacity in Cu-Al-Mn shape memory alloy, J. Alloys Compd. 821 (2020), https://doi.org/10.1016/j.jallcom.2019.153213.
[36] Y.D. Wang, L.H. Wu, P. Xue, H. Zhang, D.R. Ni, Z.Y. Ma, Improved strength with good conductivity in Cu-Cr-Zr alloys: determinant effect of under-aging treatment before rolling and aging, Materials Science and Engineering a-Structural Materials Properties Microstructure and Processing 848 (2022), https://doi.org/10.1016/j.msea.2022.143395.
[37] Y. Wu, Z. Liu, X. Qin, C. Wang, L. Zhou, Effect of initial state on hot deformation and dynamic recrystallization of Ni-Fe based alloy GH984G for steam boiler applications, J. Alloys Compd. 795 (2019) 370–384, https://doi.org/10.1016/j.jallcom.2019.05.022.
[38] S. Nagarjuna, M. Srinivas, K. Balasubramanian, D.S. Sarma, The alloy content and grain size dependence of flow stress in Cu-Ti alloys, Acta Mater. 44 (6) (1996) 2285–2293, https://doi.org/10.1016/1359-6454(95)00358-4.
[39] M. Furukawa, Y. Iwahashi, Z. Horita, M. Nemoto, N.K. Tsenev, R.Z. Valiev, T. G. Langdon, Structural evolution and the Hall-Petch relationship in an Al-Mg-Li-Zr alloy with ultra-fine grain size, Acta Mater. 45 (11) (1997) 4751–4757, https://doi.org/10.1016/S1359-6454(97)00120-1.
[40] N. Hansen, Hall–Petch relation and boundary strengthening, Scripta Mater. 51 (8) (2004) 801–806, https://doi.org/10.1016/j.scriptamat.2004.06.002.
[41] S. Fu, P. Liu, X. Chen, H. Zhou, F. Ma, W. Li, K. Zhang, Effect of aging process on the microstructure and properties of Cu-Cr-Ti alloy, Materials Science and Engineering a-Structural Materials Properties Microstructure and Processing (2021) 802, https://doi.org/10.1016/j.msea.2020.140598.
[42] J.Y. He, H. Wang, H.L. Huang, X.D. Xu, M.W. Chen, Y. Wu, X.J. Liu, T.G. Nieh, K. An, Z.P. Lu, A precipitation-hardened high-entropy alloy with outstanding tensile properties, Acta Mater. 102 (2016) 187–196, https://doi.org/10.1016/j.actamat.2015.08.076.
[43] Y. Zhang, A.A. Volinsky, H.T. Tran, Z. Chai, P. Liu, B. Tian, Y. Liu, Aging behavior and precipitates analysis of the Cu-Cr-Zr-Ce alloy, Materials Science and Engineering a-Structural Materials Properties Microstructure and Processing 650 (2016) 248–253, https://doi.org/10.1016/j.msea.2015.10.046.
[44] X. Xiao, J. Huang, J. Chen, H. Xu, Z. Li, J. Zhang, Aging behavior and precipitation analysis of Cu-Ni-Co-Si alloy, Crystals (2018), https://doi.org/10.3390/cryst8110435.
[45] Q. Lei, Z. Li, Z.-y. Pan, M.-p. Wang, Z. Xiao, C. Chen, Dynamics of phase transformation of Cu-Ni-Si alloy with super-high strength and high conductivity during aging, Trans. Nonferrous Metals Soc. China 20 (6) (2010) 1006–1011, https://doi.org/10.1016/s1003-6326(09)60249-1.